Hindawi
Journal of Nanomaterials
Volume 2019, Article ID 9710264, 13 pages
https://doi.org/10.1155/2019/9710264

Research Article

Graphene-Reinforced Biodegradable Resin Composites for Stereolithographic 3D Printing of Bone Structure Scaffolds

Zuying Feng,[1,2] **Yan Li**,[1] **Liang Hao**,[1] **Yihu Yang**,[3] **Tian Tang**,[3] **Danna Tang**,[1] **and Wei Xiong**[1]

[1]*Gemmological Institute, China University of Geosciences, Wuhan 430074, China*
[2]*Engineering Research Centre of Nano-Geomaterials of Ministry of Education, Faculty of Materials Science and Chemistry, China University of Geosciences, Wuhan 430074, China*
[3]*Shenzhen Esun Industrial Co. Ltd., Shenzhen 518000, China*

Correspondence should be addressed to Yan Li; yanli@cug.edu.cn and Liang Hao; liang_hao1972@foxmail.com

Zuying Feng and Yan Li have contributed equally to the paper.

Received 17 August 2018; Revised 3 December 2018; Accepted 24 December 2018; Published 11 April 2019

Academic Editor: Lavinia Balan

A biodegradable UV-cured resin has been fabricated via stereolithography apparatus (SLA). The formulation consists of a commercial polyurethane resin as an oligomer, trimethylolpropane trimethacrylate (TEGDMA) as a reactive diluent and phenylbis (2, 4, 6-trimethylbenzoyl)-phosphine oxide (Irgacure 819) as a photoinitiator. The tensile strength of the three-dimensional (3D) printed specimens is 68 MPa, 62% higher than that of the reference specimens (produced by direct casting). The flexural strength and modulus can reach 115 MPa and 5.8 GPa, respectively. A solvent-free method is applied to fabricate graphene-reinforced nanocomposite. Porous bone structures (a jawbone with a square architecture and a sternum with a round architecture) and gyroid scaffold of graphene-reinforced nanocomposite for bone tissue engineering have been 3D printed via SLA. The UV-crosslinkable graphene-reinforced biodegradable nanocomposite using SLA 3D printing technology can potentially remove important cost barriers for personalized biological tissue engineering as compared to the traditional mould-based multistep methods.

1. Introduction

Three-dimensional (3D) printing, also known as additive manufacturing (AM), rapid prototyping (RP), solid freeform fabrication (SFF), or layered manufacturing (LM), is an innovative technology which has been widely used in biotechnology [1], aerospace [2], medical applications [3], conductive devices [4], sensors [5], etc. 3D printing methods can be divided into five categories, including direct ink writing (DIW) [6], fused deposition modelling (FDM) [7], selective laser sintering (SLS) [8], stereolithography apparatus (SLA) [9], and three-dimensional printing (3DP) [10]. In 1986, Chales Hull invented the first 3D printer based on SLA and founded 3D Systems [11]. SLA is a layer-by-layer fabrication of 3D objects that translates liquid monomers into solid polymers utilizing ultraviolet (UV) laser to trace and cure successive layers on photosensitive resin. Compared to FDM, SLA has a higher layer resolution (~0.02 mm) [12].

Currently, most of the available commercial stereolithography resin is not biodegradable and has relatively poor mechanical property (tensile strength ~10-50 MPa). Biodegradable resins are made from renewable sources; they are relatively cheap, easy to obtain, biodegradable, and biocompatible [13], which attract broad attention. Implantable devices, tissue engineering, cell-containing hydrogels, and other biomedical engineering have been successfully fabricated from biodegradable resin through SLA [14]. Besides, 3D printing technology can achieve more complex structure and better mechanical properties, which enlarges its application in biomedical engineering. Neiman et al. [15] reported the first spatially patterned photopolymerizable polyethylene glycol-based hydrogel scaffolds coupled to a

filter (polycarbonate and polyvinylidene fluoride), which promoted cell viability and allowed for perfused culture of primary hepatocytes. Gauvin et al. [16] utilized gelatin methacrylate (GelMA) and fabricated a biological functionality scaffold by SLA. Polylactide is a biodegradable, rigid material with excellent mechanical properties, which has been successfully applied in biomedical engineering [17]. Seck et al. [18] designed a poly(ethylene glycol)/poly($_{D,L}$-lactide) (PDLLA) hydrogel structure with good mechanical properties and cell seeding characteristics for tissue engineering scaffolds by stereolithography. A porous and highly interconnected osteochondral scaffold using core-shell poly (lactic-co-glycolic) acid (PLGA) nanospheres was manufactured by SLA [19]. Great improvement (human bone marrow-derived mesenchymal stem cell adhesion, proliferation, and osteochondral differentiation) was observed in this biomimetic graded 3D printed osteochondral construct in vitro. In order to further improve the mechanical performance as well as to add some unique properties (e.g., electron conductivity, thermal conductivity, and biocompatibility), nanofillers are usually added into resin [20–23].

The performance of nanoparticle-reinforced composites can be greatly improved by the addition of nanofillers or surface modification [24–26]. As vastly reported, graphene is an emerging class of nanomaterial with ultrahigh electron conductivity (10^4 S/cm at room temperature) [27], excellent optical properties (2.3% light absorption over a broad range of wavelengths), high surface area (2630 m^2/g) [28], high mechanical properties (e.g., Young's modulus -1 TPa, tensile strength 130 GPa, respectively [27]), superior thermal conductivity (~5000 W/mK) [29], and excellent intrinsic mobility (2×10^5 cm^2/V•s, room temperature) [30]. Graphene is an important two-dimensional nanomaterial which exhibits biocompatibility as well as good electrical conductivity. Graphene-reinforced polymer is of particular interest aiming to exploit the excellent properties of graphene to produce high-performance polymer components [31, 32]. The dispersion degree of nanofillers within the polymer matrix will directly affect the final properties' improvement extent of nanocomposites [33]. Even very low filler loading could contribute to great enhancement. Graphene-based materials have been employed to manufacture conducting nanocomposites with enhanced physical and chemical properties as well as different polymers matrices, including epoxy [22], poly (methyl methacrylate) (PMMA) [34], polypropylene [35], and polystyrene [36]. Single-layer graphene possesses the best intrinsic properties; however, it is still difficult to obtain in large-scale and low cost. Moreover, its tendency to roll, scroll, fold, or wrinkle [37], unless constrained onto a solid surface, is of great concern as only a high aspect ratio, flat filler morphology does theoretically offer optimal physical property (e.g., mechanical, electrical, thermal, gas barrier, and corrosion resistance) enhancement in polymer matrix. Few layer graphene (FLG) and/or graphite nanoplatelets (GNP) might be a more viable alternative to single layer graphene as promising future nanofiller for polymer composites and coatings, if produced with good quality, cheaply, and in bulk. GNP has already been shown to provide significant improvements in mechanical properties like stiffness, strength, and surface hardness [38–41]. However, the abovementioned properties strongly depend on the number of layers stacked in the GNP, the degree of crystallinity in graphitic planes, their aspect ratio (AR), and the order of stacking [42].

However, literatures on graphene/FLG/GNP-reinforced polymer via SLA are still few [43] and graphene oxide (GO) is more commonly seen since the functional groups attached to GO make it easier to be dispersed in polymer matrix [44] and GO has good biocompatibility [45]. Manapat et al. [44] made use of the metastable, temperature-dependent characteristic of GO to improve the mechanical properties of 3D-printed commercial resin by SLA and acetone was used to disperse GO. GO-doped, gelatin–based (GelMA-PEGDA-GO) scaffolds with hierarchical structures via SLA was investigated by Zhou et al. [46]. It was found out that GO induced chondrogenic differentiation of human bone marrow mesenchymal stem cells (hMSCs), resulting in the promotion of glycosaminoglycan and collagen levels. Lim et al. [43] investigated a graphene/photopolymer resin via SLA, and Tween20 was added to disperse graphene in photopolymer resin. In order to disperse graphene in polymer, an extra solvent was usually added and this may influence the curing degree of resin.

In this present work, a UV-curable and 3D-printable and biodegradable resin has been developed. A commercial polyurethane resin was selected as oligomer with triethylene glycol dimethacrylate (TEGDMA) as reactive diluent and phenylbis (2, 4, 6-trimethylbenzoyl)-phosphine oxide (Irgacure 819) as photoinitiator. This formulation of resin has a suitable viscosity for 3D printing and stable thermal properties. This formulation fabricated by SLA has huge improvement in mechanical properties when compared with the conventional direct casting method. To further improve the properties of the prepared UV-cured resin, few layer graphene was well dispersed in the low viscosity reactive diluent and graphene-reinforced UV-cured resin was successfully fabricated via SLA. Direct 3D printing of graphene-reinforced biodegradable resin composite promises to tackle the drawbacks of traditional methods leading to a viable route to applications of multistructure graphene-modified resins. The aim of this study is to address the challenges of creating personalized complex structure for bone tissue scaffolds via SLA 3D printing. Performance of the developed resin is enhanced by using graphene-reinforced nanocomposite, showing great potential in bone tissue-engineered constructs.

2. Experimental

2.1. Materials. PLA-PUA oligomer (polylactic acid–polyurethane, made from acrylate-modified polylactide diol with a purity of 99%, $M_w = 2000–30000$, Figure 1(a)) was provided by Shenzhen Esun Industrial Co. Ltd. Phenylbis (2,4,6-trimethylbenzoyl)-phosphine oxide (Irgacure 819, green powder, Figure 1(b)) was purchased from BASF Co. Ltd. Trimethylolpropane trimethacrylate (TMPTMA), ethylene glycol dimethacrylate (EGDMA), and lauryl methacrylate (LMA) were obtained from Eternal Materials Co. Ltd.

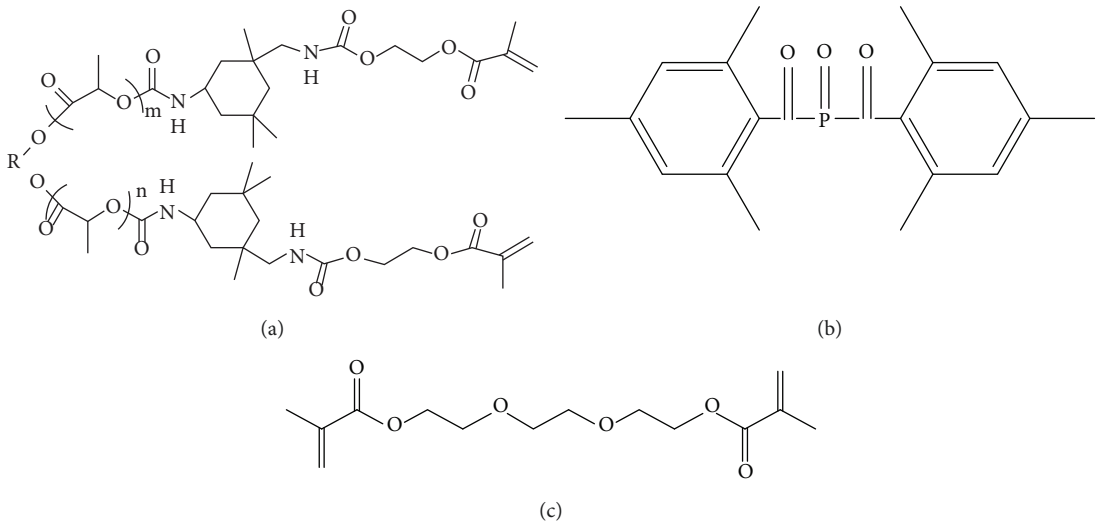

Figure 1: Chemical structures of (a) PLA-PUA oligomer, (b) Irgacure 819, and (c) TEGDMA.

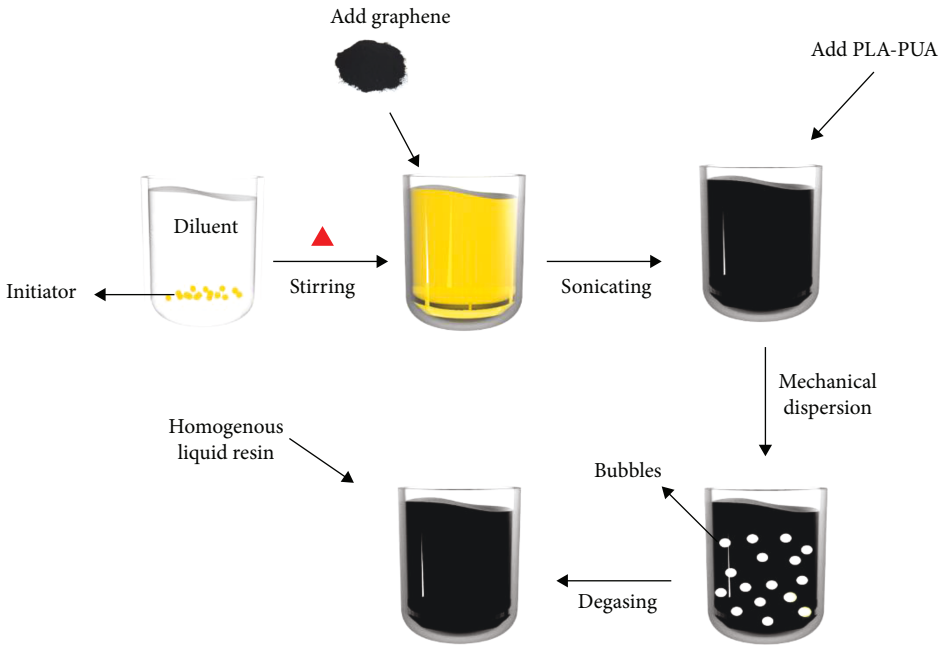

Figure 2: Schematic of the preparation process of graphene-reinforced nanocomposite.

Tripropylene glycol diacrylate (TPGDA) and trimethylolpropane triacrylate (TMPTA) were purchased from DSM Co. Ltd. Triethylene glycol dimethacrylate (TEGDMA, Figure 1(c)) and tetrahydrofurfuryl alcohol (THFA) were purchased from Sumda Material Technology Co. Ltd. The few layer graphene (1-2 μm in length, 2-5 nm in thickness) was purchased from Allightec Co. Ltd. All the raw materials were used as received.

2.2. Preparation of Liquid UV-Cured Resin. PLA-PUA was chosen as the oligomer because of its good biodegradability. Irgacure 819, as an initiator, has a high photoinitiation effect. A series of experiments were carried out to explore the compatible reactive diluent. The formulation and properties of UV-cured resin were listed in the Supplementary Materials, Table S1. Viscosity is one of the most significant factors in determining the printing quality and ranges from 0.25 to 1 Pa.s [47]. In view of the mechanical properties and other factors (curing time, smell, and hardness), the composition of 37 wt.% TEGDMA, 62 wt.% PLA-PUA, and 1 wt.% Irgacure 819 was chosen for the 3D printing after a series of experiments. Irgacure 819 powder was firstly added into TEGDMA and stirred at 30°C for 20 mins. The mixed solution was poured into PLA-PUA for further dispersion. Since there were lots of bubbles during the dispersion, a further degassing was carried out under the

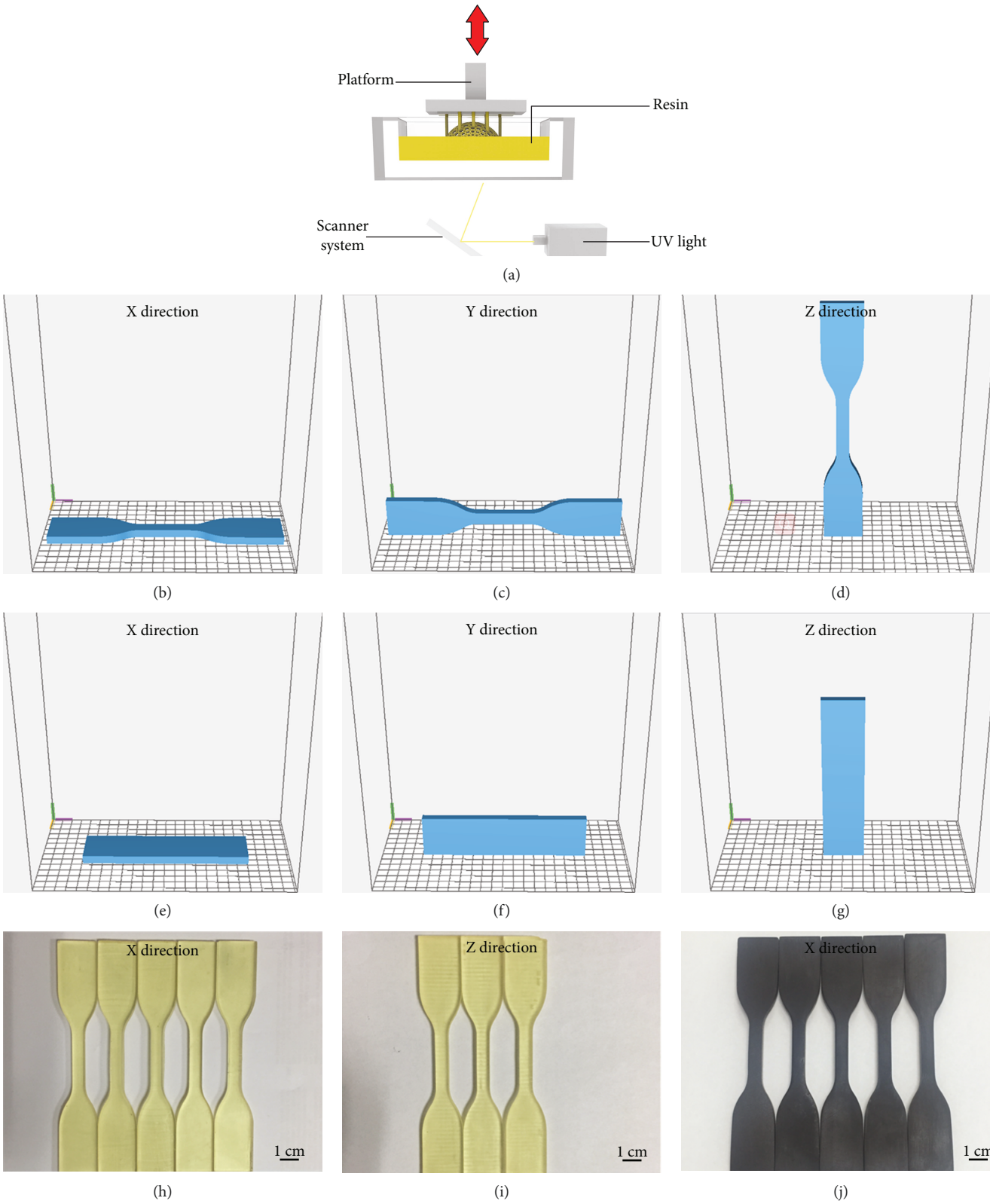

Figure 3: Continued.

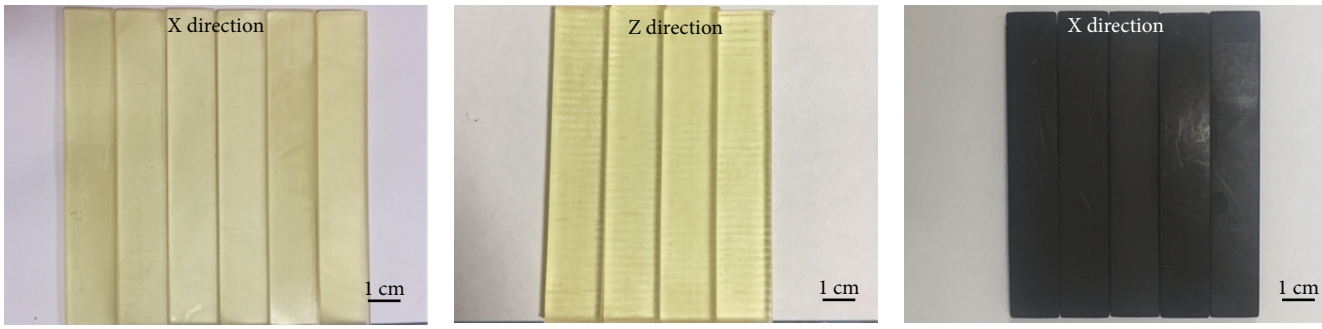

Figure 3: (a) Schematic of SLA process; (b) face up (X direction), (c) edge up (Y direction), and (d) upright (Z direction) of tensile test specimens; (e) face up (X direction), (f) edge up (Y direction), and (g) upright (Z direction) of flexural test specimens; images of tensile test specimens (h) X direction and (i) Z direction; (j) X direction specimens with graphene; images of (h) X direction and (i) Z direction (j) X direction with graphene specimens for flexural test.

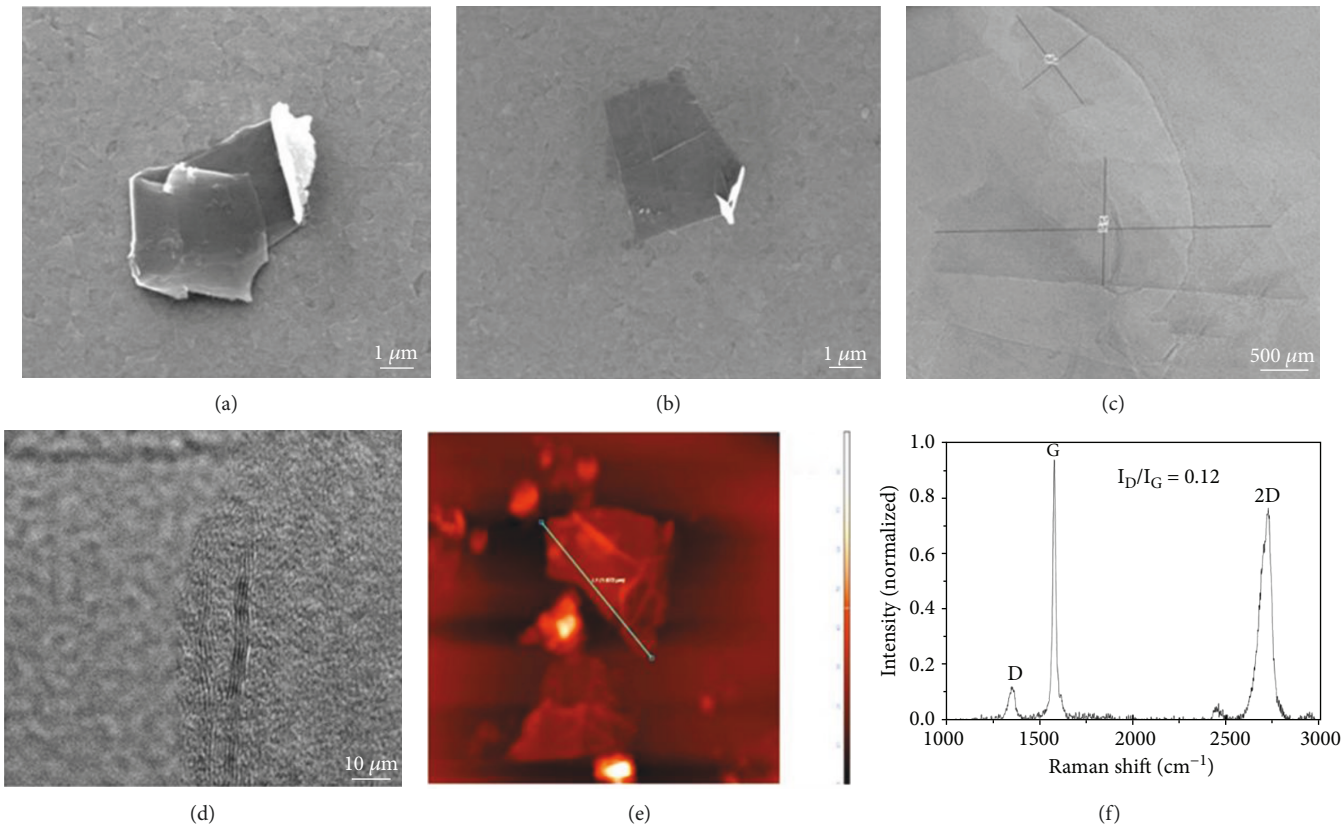

Figure 4: Representative (a, b) SEM images, (c, d) TEM, and (e) AFM images of graphene/FLG; (f) Raman image of FLG (containing D, G, and 2D peaks) confirming a graphitic structure with low defect content.

pressure of -1 bar for about 15 mins. Finally, a homogeneous liquid UV-curable resin was obtained. Graphene powder was added in the diluent after the full dissolution of the initiator. The graphene suspension was treated by ultrasonication and degassing (the subsequent process was the same as the process described above, Figure 2).

2.3. Fabrication of UV-Cured Resin by SLA. The flexural and tensile test specimens were fabricated by a 405 nm SLA (Photon, ANYCUBIC, China), respectively (see the SLA schematic in Figure 3(a)). The SLA was equipped with a 2 K liquid crystal display (LCD) masking screen (2560 × 1400 pixels) with printing accuracy of micrometres. The intensity of the UV light was set at 20 W. The print speed was 0.020 m h^{-1}. The XY resolution could reach 47 μm, and the Z axis accuracy was 1.25 μm. Rhinoceros software (version 5.0, Robert McNeel Ltd.) was utilized to build designed models. To slice the 3D file for layer-by-layer material deposition and set the

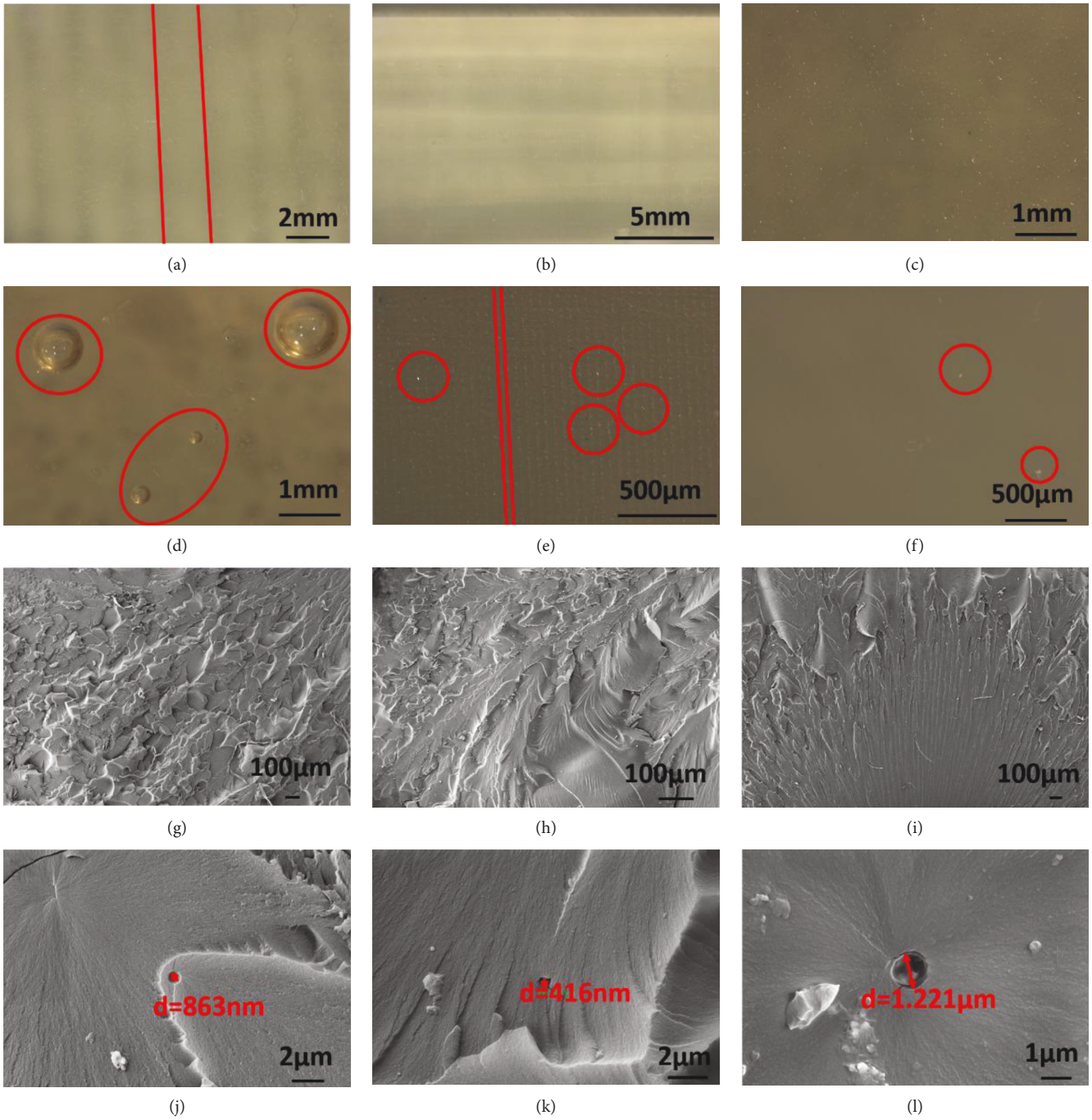

Figure 5: Optical microscopy images of (a) Z direction parallel stripes, (b) Y direction printing specimens, (c, d) direct casting reference specimens, (e) X-0.02 specimen, and (f) X-0.05 specimen; SEM images of the tensile fractured surfaces (g) X-0.02 specimen, (h) X-0.05 specimen, (i) direct casting reference specimen, (j) bubble in X-0.02 specimen, (k) bubble in X-0.05 specimen, and (l) bubble in direct casting reference specimen (d represents diameter of the bubble).

various parameters during printing, ANYCUBIC Photon Slicer software (China, ANYCUBIC Ltd.) was utilized. All specimens were labelled as M-n; M and n represented the direction of printing and the layer thickness, respectively. There were three diverse printing directions (Figures 3(b)–3(g)). For example, X-0.02 means the specimens printed at X direction with the thickness of 0.02 mm each layer. The reference specimens by direct casting method were also prepared for comparison (Supplementary Materials, Figure S1). X-0.05 mm tensile and flexural specimens with 0.5 wt.% graphene were also fabricated (Figures 3(j) and 3(m)).

2.4. Characterisations

2.4.1. Morphological Analysis. The morphology of cross-section areas of the specimens coated with gold after

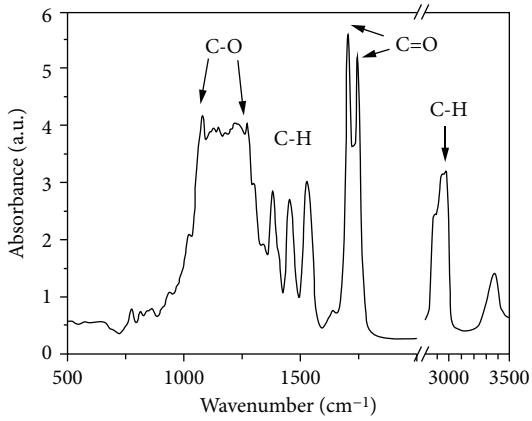

Figure 6: FTIR spectra of UV-cured resin.

Table 1: The viscosity of different resin.

Materials	Viscosity at 25°C (mPa.s)	Viscosity at 30°C (mPa.s)	Refs
PEGGEA/TMPTA (7 : 3)	<200	—	[49]
Urethane acrylate oligomer	≈375	—	[63]
PDLLA	≈1000	—	[58]
Renshape™ SL7545	—	350	[47]
SL7560	—	197	[64]
PLA-PUA/TEGDMA	504	281	This study
PLA-PUA/TEGDMA/ graphene	847	500	

mechanical test (Supplementary Materials, Figure S2) was observed by a scanning electron microscopy (SEM, ZEISS Sigma 300, Germany) with an acceleration voltage of 15 kV. SEM was conducted to assess the morphology and in particular the length (defined as the longest lateral dimension) of the graphene, FLG, GNP. Please refer to our previous publication for more information [21]. Optical microscope (OM, Leica M205 A, Germany) was applied to observe the surface appearance and the distribution of bubbles.

Transmission electron microscopy (TEM) (JOEL JEM-2010, Japan) was used to see the morphology of graphene/FLG/GNP particles. Please refer to our previous publications for more information [21, 48]. The thickness of the GNP particles is estimated from the thickness of the edge of the particles sticking out of the plane of the copper grid.

Atomic force microscopy (AFM, NT-MDT NTegra, Russia) was also used to study the morphology of graphene flakes. AFM probes (Point Probe Plus Silicon—SPM sensor, type: PPP-FMR-10, force constant: 0.5-9.8 N/m) were purchased from Nanosensors™. Typically, a small amount of particle was immersed in acetone to a final concentration less than 0.5 mg•ml^{-1}. The AFM samples were prepared by drop casting a diluted graphene/acetone dispersion on a mica substrate. After evaporation of acetone, the specimens were scanned as prepared.

Raman spectroscopy (Nicolet Almega XR, Thermo Fisher Scientific, USA) was utilized to characterise the graphene flakes. "Graphene sheets" were prepared by vacuum filtration of the dispersion through a porous membrane (PVDF, pore size 0.45 μm). Raman measurements were performed with a wavelength of 532 nm.

2.5. Viscosity Test. The viscosity of the liquid UV-cured resin was tested by the viscometer (LV DV-II+Pro, America) with the temperature and rotation speed in the range of 25 to 50°C and 6 to 60 rpm, respectively.

2.5.1. Thermogravimetric Analysis. Thermalgravimetric analyser (TG-DTA, Model STA449F3, Germany) was utilized and the temperature was ramped up at 5°C•min^{-1} from 30 to 500°C under nitrogen atmosphere.

2.5.2. Surface Characterisation. Drop shape analyser (DSA, JC2000C1, Shanghai Zhongchen Digital Technic Apparatus Co. Ltd.) was utilized to measure the contact angle by sessile drop method. A syringe squeezed a drop of water on the surface of UV-cured resin vertically. The image of water contact angle was recorded after 5 seconds. Surface tension was obtained from a tension meter (JK99B, Shanghai Zhongchen Digital Technic Apparatus Co. Ltd.).

2.5.3. Mechanical Properties. Mechanical test was conducted by a 10 KN microcomputer control electronic universal testing machine (Instron, CMT4104, China). The flexural test samples were fabricated via a 3D printer with dimensions of $3.2 \times 12.7 \times 70$ mm^3 according to the ASTM-D 790 standard. The support span to depth ratio was 16 : 1 while the cross-head speed was calculated in accordance to ASTM-D 790 with the strain rate 0.01 mm/mm/min. Tensile test specimens were prepared in accordance with ASTM-D 638 (Figure 3(h), type IV) utilizing a test speed of 5 mm•min^{-1}. The surfaces of the specimens were artificial slightly polished with different grade abrasive paper (from 1000 to 4000 grit).

2.5.4. FTIR. Fourier transform infrared spectroscopy (FTIR, VERTEX 80, Germany) was used to determine the chemical structure of UV-cured resin.

2.5.5. Volume Shrinkage Rate. Hydrostatic balance (BSA 223S, China) was applied to measure the density of UV-cured resin. The volume shrinkage (S_v) was calculated according to equation (1) [49].

$$S_v = \frac{\rho_1 - \rho_2}{\rho_1} \times 100\%, \quad (1)$$

where ρ_1 and ρ_2 are the density of the UV-cured resin and liquid UV-cured resin, respectively.

3. Results and Discussion

3.1. Morphological Analysis of Graphene. SEM images in Figures 4(a) and 4(b) present the typical morphology of the graphene flakes used in this study. The average graphene or few layer graphene (FLG) was around 1.52 ± 0.35 μm, while

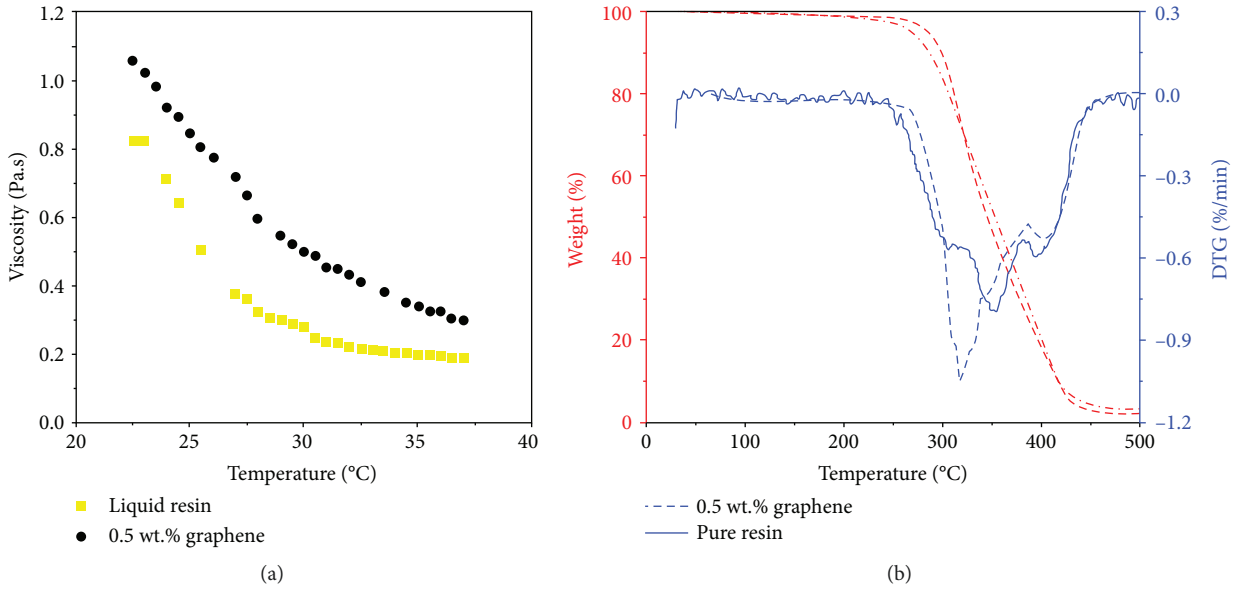

Figure 7: (a) The viscosities of liquid resin with or without graphene at different temperatures. (b) TGA and DTG curves of UV-cured resin with or without graphene.

Table 2: Volume shrinkage rates of different layer thickness 3D printing parameters.

Layer thickness (mm)	Density (g/cm^3)	Volume shrinkage rate (%)
0.02	1.166	6.27
0.05	1.170	6.59
0.1	1.172	6.75
0.15	1.172	6.75
0.2	1.173	6.83

the thickness was ~3 nm (aspect ratio ≈500). The edges of the graphene sheets (Figures 4(c) and 4(d)) indicated at graphene and FLG were obtained without aggregation after liquid phase probe sonication. AFM image and Raman data (Figures 4(e) and 4(f)) confirm that FLG was obtained. Moreover, Raman spectroscopy (Figure 4(f)) of FLG (containing D, G, and 2D peaks) confirmed a graphitic structure with low defect content.

3.2. Morphological and FTIR Analysis of the UV-Curable Resin. In order to further explore the relationship between bubbles and mechanical properties, optical microscopy was observed (Figures 5(a)–5(f)). Figures 5(c) and 5(d) specifically demonstrated lots of bubbles with big size (max. to 1 mm) existed in the direct casting reference specimens, deteriorating the mechanical properties. Besides, there were more bubbles in X-0.05 specimens than X-0.02 specimens (Figures 5(e) and 5(f)). Z direction was not recommended for 3D printing because of the distinct and continuous fringes on the surface caused by the motion of Z axis (Figures 3(i)–3(l)). SEM images of tensile fractured surface of PLA-PUA/-TEGDMA composites were analysed, with the purpose of exploring the mechanism in mechanical properties. From overall view of the fracture surface of X-0.02 and X-0.05 specimens, the cracking direction was disordered and fracture surface was rougher (Figures 5(g) and 5(h)) compared to that of the direct casting reference specimens (Figure 5(i)), which is a typical brittle fracture with smooth and orderly fracture surface. However, the mechanical properties of the developed resin are still much higher than commercial resin for 3D printing, demonstrated by the following tests. The 3D printed specimens may prevent the macrocracking propagation causing the fracture surface disorder, consuming energy in the process of fracture, and leading to a better mechanical property. What is more, the number and size of bubbles or defects also relatively decreased a lot (Figures 5(j)–5(l)). Largest bubbles appeared in direct casting reference specimens, leading to poor mechanical properties.

The chemical structure of UV-cured resin could be derived from FTIR analysis (Figure 6). In the low wavenumber spectral region, namely, the stretching signals of C-O corresponding to ester group at 1080 and 1270 cm^{-1}, the bending of C-H at 1454 cm^{-1}, and the stretching vibrations of C=O at 1703 cm^{-1} and 1743 cm^{-1} could be clearly observed. Besides, in the high wavenumber spectral region, relevant bonds corresponding to C-H and N-H stretching at 2977 cm^{-1} and 3374 cm^{-1} could be noticed. The characteristic peak of isocyanate functional group disappeared in the spectrum [50], while the stretching vibration of N-O was observed at 1529 cm^{-1}. This change indicated the polyurethane resin completely reacted with the diluent.

3.3. Effect Parameters on 3D Printing. The viscosity is a decisive parameter affecting 3D printing. High viscosity may lead to deformation or failure. This developed resin formulation

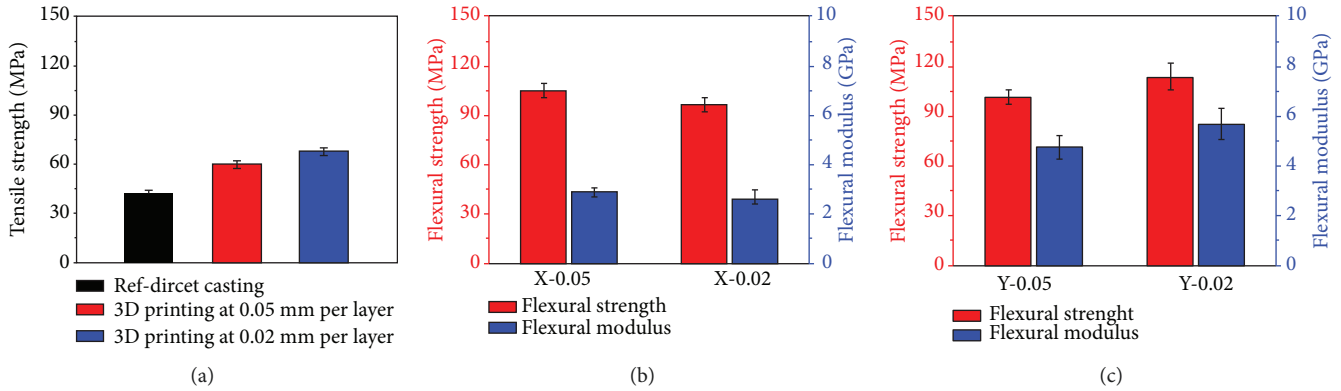

Figure 8: (a) Tensile strength of direct casting reference, X-0.05 and X-0.02 specimens; flexural strength and modulus of (b) X-0.05 and X-0.02 specimens and (c) Y-0.05 and Y-0.02 specimens.

has a suitable viscosity for SLA processing (Table 1) and a relatively low viscosity (from 0.25 to 1 Pa.s) is required for SLA 3D printing. The viscosity decreased with the temperature increasing (Figure 7(a)) and almost reached a plateau after the temperature surpassed 35°C. The addition of 0.5 wt.% graphene led to an increase in liquid resin viscosity. The viscosity of liquid resin without or with graphene was approximately 0.504 Pa.s and 0.847 Pa.s at 25°C, which is suitable for SLA processing.

Surface tension and water contact angle (see Figure S3 in the Supplementary Materials) of the liquid resin were 37 mN m^{-1} and 76°, showing the hydrophobicity of the material. To enhance the adhesion of cell, surface functionalization had been applied in tissue engineering scaffolds [51, 52]. After adding 0.5 wt.% graphene into liquid resin, the surface tension and water contact angle were increased to 41 mN m^{-1} and 82°, respectively. However, researches showed hybrid hydrophobic and hydrophilic scaffold was less cytotoxic and more biocompatible [53].

The thermal stability of UV-cured resin was analysed in nitrogen atmosphere with temperature ranging from 30 to 500°C (Figure 7(b)). The UV-cured resin was thermally stable below 200°C. As temperature increased, a rapid weight loss appeared at 250°C, corresponding to the fragmentation of the macromolecules and disproportionation and gasification processes. The weight of the UV-cured resin was kept constant above 430°C, indicating the finish of the decomposition. The degradation temperature of graphene-reinforced nanocomposite is higher than resin reference, showing that the addition of graphene could enhance the thermal stability of graphene-modified resin.

3.4. Mechanical Properties. The density of the UV-cured resin increased with the enhancing layer thickness as well as the volume shrinkage rate. The thinner the thickness was, the better the printing accuracy achieved. The volume shrinkage rate of PLA-PUA/TEGDMA resin was 6% (Table 2) due to the formation of a high cross-linking. Because the high concentration double bonds in low molecular weight of TEGDMA monomers converted to single bonds, the intermolecular distance reduced in the polymerization resulting in high volume shrinkage [54, 55]. The decrease in accuracy owing to volume shrinkage rate could be compensated by setting the dimensions in advance. In addition, the adding of nonreactive inorganic fillers can significantly reduce the volume shrinkage rate [56]. Considering the existing problem of volume shrinkage affecting the accuracy, the layer thickness of 0.02 mm and 0.05 mm was investigated.

Table 3: Mechanical properties of different resin fabricated by SLA.

Materials	Tensile strength (MPa)	Flexural strength (MPa)	Flexural modulus (GPa)	Refs
PEGDA/UDMA (1 : 4)	—	95	2.2	[65]
Hydroxyapatite powder filled TTA/HEMA (4 : 1)	—	70	8.0	
SL7560	44	—	—	[64]
Somos 7110 resin	51	—	—	[66]
SiO_2 5% *w/w*	54	—	—	[67]
OMMT 1% *w/w*	47	—	—	
ATP 1% *w/w*	41	—	—	
PDLLA	—	94	2.9	[58]
PLA-PUA/TEGDMA	68	115	5.8	this study

The printing accuracy has a close relationship with the mechanical properties (Figure 8). Specimens manufactured through the conventional method (direct casting) showed relatively poor mechanical properties because of vast visible bubbles and defects. As revealed in Figure 8(a), the tensile strength of direct casting reference specimens was around 41.8 ± 2.1% MPa. The existence of bubbles may affect the mechanical properties. Even if degassing is carried out, the numerous bubbles are still inevitable when the liquid resin is casted into the mould. The tensile strength of the X-0.05 and X-0.02 3D printing specimens was 43% and 62% higher than that of the direct casting reference specimens, respectively. What is more, the thinner the layer thickness was, the lesser the bubbles in the specimens. However, the flexural strength and flexural modulus of X-0.05 specimens (average thickness: 2.67 mm) were a little higher than that of the X-0.02 specimens (average

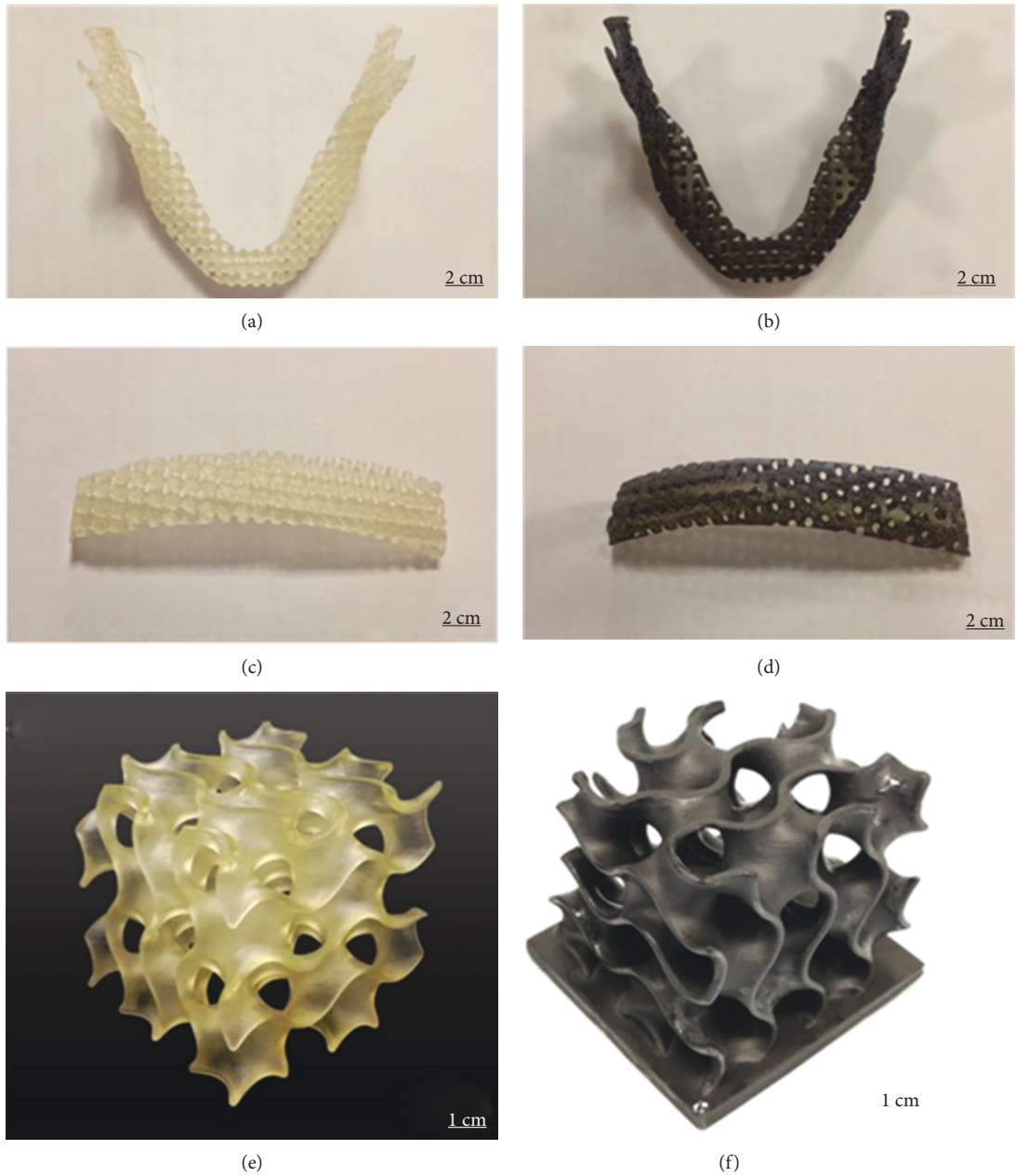

Figure 9: Images of (a) pure UV-cured resin and (b) graphene-reinforced nanocomposite jawbone with a square architecture. Images of (c) pure UV-cured resin and (d) graphene-reinforced nanocomposite sternum with a round architecture. Images of (e) pure UV-cured resin and (f) graphene-reinforced nanocomposite gyroid scaffold for bone tissue engineering.

thickness: 3.48 mm) (Figure 8(b)). Since the different volume shrinkage was in the Z axis (Table 2), the thickness of X-0.02 specimens was thicker than that of X-0.05 specimens.

The width of the specimens was reduced when printed at Y direction because of shrinkage. The thickness of Y-0.05 specimens was equal to that of Y-0.02 specimens, namely, layer thickness decided the number of bubbles and defects in the specimens. So there were much smaller bubbles and other defects in Y-0.02 specimens. That was why Y-0.02 possessed a better flexural strength and flexural modulus than Y-0.05 (Figure 8(c), see Table S2–S7 in the Supplementary Materials for the dimensions of all the specimens). The comparison of the experimental results and the representative data from literature was summarized in Table 3.

With such good mechanical properties, this UV-cured resin can be used for the application of preparing porous bone structures (Figures 9(a)–(d)) and scaffold (Figures 9(e) and 9(f)) by SLA. A jawbone with a square architecture and a sternum with a round architecture were fabricated. A commercial UV-curable resin with a tensile strength of only 23.4 MPa was also able to prepare the sternum (Supplementary Materials, Figure S4). 3D scaffold architecture has been investigated by many researches, and modulus of these scaffolds ranged from 0.1 to 22 MPa [16, 19, 57]. The flexural strength and modulus of a PDLLA-based scaffold were

94 MPa and 2.9 GPa, respectively [58]. Hydroxyapatite has a similar composition to the human bone, and it was added into a UV-curable epoxy resin for the fabrication of bone tissue engineering [59]. Compared to PLA-PUA, UV-curable epoxy resin has high viscosity and poor durability [60]. The mechanical properties of this PLA-PUA/TEGDMA material were close or even better than the previous work. With the aid of SLA, the bone structure or scaffold can be individually personalized and available for clinic applications, which can save abundant cost and time of both medical personnel and patient [61, 62]. It is promising for PLA-PUA/TEGDMA material to be applied in bone tissue engineering.

4. Conclusions

A UV-curable resin based on PLA-PUA and TEGDMA was well developed and successfully printed via SLA, and the formulation had a suitable viscosity window for SLA processing. Layer thickness determined the printing resolution and influenced the mechanical properties of the printed specimens. Generally speaking, the thinner of the printing layer thickness, the higher the resolution and mechanical properties of the specimens. The tensile strength of the X-0.05 and X-0.02 specimens was 43% and 62% higher than that of the direct casting reference specimens. Layer thickness also affected the number, size, and distribution of bubbles and other defects in the specimens. A solvent-free method to fabricate graphene-reinforced nanocomposite was developed by dispersing graphene directly into TEGDMA. A jawbone with a square architecture and a sternum with a round architecture and gyroid scaffold of graphene-modified nanocomposite for bone tissue engineering were fabricated via SLA. This developed UV-curable resin formulation with high mechanical properties has great potential of application in biological engineering; what is more, the performance can be further improved by nanofillers and surface modification.

Data Availability

The data used to support the findings of this study are available from the corresponding author upon request.

Additional Points

Highlights. (1) A new formulation of a biodegradable UV-curable resin with graphene loading applied in stereolithography has been developed. (2) The formulation of biodegradable UV-curable resin exhibits good mechanical properties. (3) Porous bone structures of PLA-PUA/TEGDMA resin show great potential in tissue engineering

Conflicts of Interest

The authors declare that there is no conflict of interest regarding the publication of this paper.

Authors' Contributions

Ms. Zuying Feng and Dr. Yan Li have contributed equally to the paper.

Acknowledgments

The authors gratefully acknowledge the financial support from Esun Co. Ltd. The project was kindly supported by the Fundamental Research Funds for the Central Universities, China University of Geosciences (Wuhan) (no. CUG170677).

Supplementary Materials

Figure S1: photograph of (a) direct casting specimens. Figure S2: optical images of the tensile fractured lateral view: (g) X-0.02 specimen, (h) X-0.05 specimen, and (i) direct casting specimen. Figure S3: water contact angles of UV-cured resin. Figure S4: images of sternum with a round architecture using a commercial resin: (a) photography (b) and optical microscopy image. Table S1: the formulation and physical properties of the UV-cured resin. Table S2: the dimensions of tensile test X-0.02 specimens. Table S3: the dimensions of tensile test X-0.05 specimens. Table S4: the dimensions of flexural test X-0.02 specimens. Table S5: the dimensions of flexural test X-0.05 specimens. Table S6: the dimensions of flexural test Y-0.02 specimens. Table S7: the dimensions of flexural test Y-0.05 specimens. *(Supplementary Materials)*

References

[1] H. Ma, J. Luo, Z. Sun et al., "3D printing of biomaterials with mussel-inspired nanostructures for tumor therapy and tissue regeneration," *Biomaterials*, vol. 111, pp. 138–148, 2016.

[2] C. R. Rambo, N. Travitzky, K. Zimmermann, and P. Greil, "Synthesis of TiC/Ti–Cu composites by pressureless reactive infiltration of TiCu alloy into carbon preforms fabricated by 3D-printing," *Materials Letters*, vol. 59, no. 8-9, pp. 1028–1031, 2005.

[3] F. Rengier, A. Mehndiratta, H. von Tengg-Kobligk et al., "3D printing based on imaging data: review of medical applications," *International Journal of Computer Assisted Radiology and Surgery*, vol. 5, no. 4, pp. 335–341, 2010.

[4] G. Postiglione, G. Natale, G. Griffini, M. Levi, and S. Turri, "Conductive 3D microstructures by direct 3D printing of polymer/carbon nanotube nanocomposites via liquid deposition modeling," *Composites Part A: Applied Science and Manufacturing*, vol. 76, pp. 110–114, 2015.

[5] S. J. Leigh, C. P. Purssell, J. Bowen, D. A. Hutchins, J. A. Covington, and D. R. Billson, "A miniature flow sensor fabricated by micro-stereolithography employing a magnetite/acrylic nanocomposite resin," *Sensors and Actuators A: Physical*, vol. 168, no. 1, pp. 66–71, 2011.

[6] A. E. Jakus, E. B. Secor, A. L. Rutz, S. W. Jordan, M. C. Hersam, and R. N. Shah, "Three-dimensional printing of high-content graphene scaffolds for electronic and biomedical applications," *ACS Nano*, vol. 9, no. 4, pp. 4636–4648, 2015.

[7] N. Guo and M. C. Leu, "Additive manufacturing: technology, applications and research needs," *Frontiers of Mechanical Engineering*, vol. 8, no. 3, pp. 215–243, 2013.

[8] E. O. Olakanmi, R. F. Cochrane, and K. W. Dalgarno, "A review on selective laser sintering/melting (SLS/SLM) of aluminium alloy powders: processing, microstructure, and properties," *Progress in Materials Science*, vol. 74, pp. 401–477, 2015.

[9] L. Elomaa, S. Teixeira, R. Hakala, H. Korhonen, D. W. Grijpma, and J. V. Seppala, "Preparation of poly(ε-caprolactone)-based tissue engineering scaffolds by stereolithography," *Acta Biomaterialia*, vol. 7, no. 11, pp. 3850–3856, 2011.

[10] A. Azhari, E. Marzbanrad, D. Yilman, E. Toyserkani, and M. A. Pope, "Binder-jet powder-bed additive manufacturing (3D printing) of thick graphene-based electrodes," *Carbon*, vol. 119, pp. 257–266, 2017.

[11] B. C. Gross, J. L. Erkal, S. Y. Lockwood, C. Chen, and D. M. Spence, "Evaluation of 3D printing and its potential impact on biotechnology and the chemical sciences," *Analytical Chemistry*, vol. 86, no. 7, pp. 3240–3253, 2014.

[12] H. Lin, D. Zhang, P. G. Alexander et al., "Application of visible light-based projection stereolithography for live cell-scaffold fabrication with designed architecture," *Biomaterials*, vol. 34, no. 2, pp. 331–339, 2013.

[13] S. Rengasamy and V. Mannari, "Development of soy-based UV-curable acrylate oligomers and study of their film properties," *Progress in Organic Coatings*, vol. 76, no. 1, pp. 78–85, 2013.

[14] F. P. W. Melchels, J. Feijen, and D. W. Grijpma, "A review on stereolithography and its applications in biomedical engineering," *Biomaterials*, vol. 31, no. 24, pp. 6121–6130, 2010.

[15] J. A. Shepard Neiman, R. Raman, V. Chan et al., "Photopatterning of hydrogel scaffolds coupled to filter materials using stereolithography for perfused 3D culture of hepatocytes," *Biotechnology and Bioengineering*, vol. 112, no. 4, pp. 777–787, 2015.

[16] R. Gauvin, Y. C. Chen, J. W. Lee et al., "Microfabrication of complex porous tissue engineering scaffolds using 3D projection stereolithography," *Biomaterials*, vol. 33, no. 15, pp. 3824–3834, 2012.

[17] F. P. W. Melchels, K. Bertoldi, R. Gabbrielli, A. H. Velders, J. Feijen, and D. W. Grijpma, "Mathematically defined tissue engineering scaffold architectures prepared by stereolithography," *Biomaterials*, vol. 31, no. 27, pp. 6909–6916, 2010.

[18] T. M. Seck, F. P. W. Melchels, J. Feijen, and D. W. Grijpma, "Designed biodegradable hydrogel structures prepared by stereolithography using poly(ethylene glycol)/poly(d,l-lactide)-based resins," *Journal of Controlled Release*, vol. 148, no. 1, pp. 34–41, 2010.

[19] N. J. Castro, J. O'Brien, and L. G. Zhang, "Integrating biologically inspired nanomaterials and table-top stereolithography for 3D printed biomimetic osteochondral scaffolds," *Nanoscale*, vol. 7, no. 33, pp. 14010–14022, 2015.

[20] M. Raimondo, L. Guadagno, V. Speranza, L. Bonnaud, P. Dubois, and K. Lafdi, "Multifunctional graphene/POSS epoxy resin tailored for aircraft lightning strike protection," *Composites Part B: Engineering*, vol. 140, pp. 44–56, 2018.

[21] Y. Li, H. Zhang, M. Crespo et al., "In situ exfoliation of graphene in epoxy resins: a facile strategy to efficient and large scale graphene nanocomposites," *ACS Applied Materials & Interfaces*, vol. 8, no. 36, pp. 24112–24122, 2016.

[22] Y. Li, H. Zhang, H. Porwal, Z. Huang, E. Bilotti, and T. Peijs, "Mechanical, electrical and thermal properties of in-situ exfoliated graphene/epoxy nanocomposites," *Composites Part A: Applied Science and Manufacturing*, vol. 95, pp. 229–236, 2017.

[23] Y. Li, H. Zhang, Y. Liu et al., "Synergistic effects of spray-coated hybrid carbon nanoparticles for enhanced electrical and thermal surface conductivity of CFRP laminates," *Composites Part A: Applied Science and Manufacturing*, vol. 105, pp. 9–18, 2018.

[24] C. Ingrosso, C. Esposito Corcione, R. Striani et al., "UV-curable nanocomposite based on methacrylic-siloxane resin and surface-modified TiO2 nanocrystals," *ACS Applied Materials & Interfaces*, vol. 7, no. 28, pp. 15494–15505, 2015.

[25] H. Cui and M. R. Kessler, "Pultruded glass fiber/bio-based polymer: Interface tailoring with silane coupling agent," *Composites Part A: Applied Science and Manufacturing*, vol. 65, pp. 83–90, 2014.

[26] P. Christian, I. A. Jones, C. D. Rudd, R. I. Campbell, and T. J. Corden, "Monomer transfer moulding and rapid prototyping methods for fibre reinforced thermoplastics for medical applications," *Composites Part A: Applied Science and Manufacturing*, vol. 32, no. 7, pp. 969–976, 2001.

[27] S. R. Shin, Y. C. Li, H. L. Jang et al., "Graphene-based materials for tissue engineering," *Advanced Drug Delivery Reviews*, vol. 105, Part B, pp. 255–274, 2016.

[28] L. Zhang, F. Zhang, X. Yang et al., "Porous 3D graphene-based bulk materials with exceptional high surface area and excellent conductivity for supercapacitors," *Scientific Reports*, vol. 3, no. 1, p. 1408, 2013.

[29] A. S. Nissimagoudar and N. S. Sankeshwar, "Electronic thermal conductivity and thermopower of armchair graphene nanoribbons," *Carbon*, vol. 52, pp. 201–208, 2013.

[30] X.-S. Ye, Z.-G. Shao, H. Zhao, L. Yang, and C.-L. Wang, "Intrinsic carrier mobility of germanene is larger than graphene's: first-principle calculations," *RSC Advances*, vol. 4, no. 41, pp. 21216–21220, 2014.

[31] F. Conrado and M. Pavese, "A continuous 3d-graphene network to overcome threshold issues and contact resistance in thermally conductive graphene nanocomposites," *Journal of Nanomaterials*, vol. 2017, Article ID 8974174, 11 pages, 2017.

[32] M. Y. Shen, T. Y. Chang, T. H. Hsieh et al., "Mechanical properties and tensile fatigue of graphene nanoplatelets reinforced polymer nanocomposites," *Journal of Nanomaterials*, vol. 2013, Article ID 565401, 9 pages, 2013.

[33] J. Wei, R. Atif, T. Vo, and F. Inam, "Graphene nanoplatelets in epoxy system: dispersion, reaggregation, and mechanical properties of nanocomposites," *Journal of Nanomaterials*, vol. 2015, Article ID 561742, 12 pages, 2015.

[34] J. Song, J. Zhang, and C. Lin, "Influence of graphene oxide on the tribological and electrical properties of PMMA composites," *Journal of Nanomaterials*, vol. 2013, Article ID 846102, 5 pages, 2013.

[35] S. Zhao, F. Chen, C. Zhao, Y. Huang, J. Y. Dong, and C. C. Han, "Interpenetrating network formation in isotactic polypropylene/graphene composites," *Polymer*, vol. 54, no. 14, pp. 3680–3690, 2013.

[36] Y. Li, H. Porwal, Z. Huang, H. Zhang, E. Bilotti, and T. Peijs, "Enhanced thermal and electrical properties of polystyrene-graphene nanofibers via electrospinning," *Journal of Nanomaterials*, vol. 2016, Article ID 4624976, 8 pages, 2016.

[37] R. J. Young, I. A. Kinloch, L. Gong, and K. S. Novoselov, "The mechanics of graphene nanocomposites: a review," *Composites Science and Technology*, vol. 72, no. 12, pp. 1459–1476, 2012.

[38] B. Das, K. Eswar Prasad, U. Ramamurty, and C. N. R. Rao, "Nano-indentation studies on polymer matrix composites reinforced by few-layer graphene," *Nanotechnology*, vol. 20, no. 12, 2009.

[39] U. Maitra, K. E. Prasad, U. Ramamurty, and C. N. R. Rao, "Mechanical properties of nanodiamond-reinforced polymer-matrix composites," *Solid State Communications*, vol. 149, no. 39-40, pp. 1693–1697, 2009.

[40] H. Kim, A. A. Abdala, and C. W. Macosko, "Graphene/polymer nanocomposites," *Macromolecules*, vol. 43, no. 16, pp. 6515–6530, 2010.

[41] H. Porwal, S. Grasso, and M. J. Reece, "Review of graphene–ceramic matrix composites," *Advances in Applied Ceramics*, vol. 112, no. 8, pp. 443–454, 2013.

[42] R. Sengupta, M. Bhattacharya, S. Bandyopadhyay, and A. K. Bhowmick, "A review on the mechanical and electrical properties of graphite and modified graphite reinforced polymer composites," *Progress in Polymer Science*, vol. 36, no. 5, pp. 638–670, 2011.

[43] S. M. Lim, B. S. Shin, and K. Kim, "Characterization of products using additive manufacturing with graphene/photopolymer-resin nano-fluid," *Journal of Nanoscience and Nanotechnology*, vol. 17, no. 8, pp. 5492–5495, 2017.

[44] J. Z. Manapat, J. D. Mangadlao, B. D. B. Tiu, G. C. Tritchler, and R. C. Advincula, "High-strength stereolithographic 3D printed nanocomposites: graphene oxide metastability," *ACS Applied Materials & Interfaces*, vol. 9, no. 11, pp. 10085–10093, 2017.

[45] K. Wang, J. Ruan, H. Song et al., "Biocompatibility of graphene oxide," *Nanoscale Research Letters*, vol. 6, 2010.

[46] X. Zhou, M. Nowicki, H. Cui et al., "3D bioprinted graphene oxide-incorporated matrix for promoting chondrogenic differentiation of human bone marrow mesenchymal stem cells," *Carbon*, vol. 116, pp. 615–624, 2017.

[47] B. W. Huang, G. L. Cheng, C. Deng, and H. H. Zou, "Investigation on some properties of Renshape™ SL7545 type photosensitive resin and its application for stereolithography material," *Applied Mechanics and Materials*, vol. 252, pp. 220–223, 2012.

[48] H. Zhang, Y. Liu, S. Huo et al., "Filtration effects of graphene nanoplatelets in resin infusion processes: problems and possible solutions," *Composites Science and Technology*, vol. 139, pp. 138–145, 2017.

[49] X. Wei, D. Li, W. Jiang et al., "3D printable graphene composite," *Scientific Reports*, vol. 5, no. 1, p. 11181, 2015.

[50] A. Karmarkar, S. S. Chauhan, J. M. Modak, and M. Chanda, "Mechanical properties of wood–fiber reinforced polypropylene composites: effect of a novel compatibilizer with isocyanate functional group," *Composites Part A: Applied Science and Manufacturing*, vol. 38, no. 2, pp. 227–233, 2007.

[51] Y. Cai, J. Li, C. K. Poh et al., "Collagen grafted 3D polycaprolactone scaffolds for enhanced cartilage regeneration," *Journal of Materials Chemistry B*, vol. 1, no. 43, 2013.

[52] S. Jo, S. M. Kang, S. A. Park, W. D. Kim, J. Kwak, and H. Lee, "Enhanced adhesion of preosteoblasts inside 3D PCL scaffolds by polydopamine coating and mineralization," *Macromolecular Bioscience*, vol. 13, no. 10, pp. 1389–1395, 2013.

[53] E. J. P. Jansen, R. E. J. Sladek, H. Bahar et al., "Hydrophobicity as a design criterion for polymer scaffolds in bone tissue engineering," *Biomaterials*, vol. 26, no. 21, pp. 4423–4431, 2005.

[54] L. C. Yamasaki, A. G. de Vito Moraes, M. Barros et al., "Polymerization development of "low-shrink" resin composites: reaction kinetics, polymerization stress and quality of network," *Dental Materials*, vol. 29, no. 9, pp. e169–e179, 2013.

[55] W. Zhang, H. Dong, T. Zhang, J. Guo, and J. Wei, "The effect of monomer structures on photopolymerization kinetics and volume shrinkage behavior for plasma display panel barrier rib," *Journal of Applied Polymer Science*, vol. 125, no. 1, pp. 77–87, 2012.

[56] T. Spinell, A. Schedle, and D. C. Watts, "Polymerization shrinkage kinetics of dimethacrylate resin-cements," *Dental Materials*, vol. 25, no. 8, pp. 1058–1066, 2009.

[57] C. G. Jeong and S. J. Hollister, "A comparison of the influence of material on in vitro cartilage tissue engineering with PCL, PGS, and POC 3D scaffold architecture seeded with chondrocytes," *Biomaterials*, vol. 31, no. 15, pp. 4304–4312, 2010.

[58] F. P. W. Melchels, J. Feijen, and D. W. Grijpma, "A poly(D,L-lactide) resin for the preparation of tissue engineering scaffolds by stereolithography," *Biomaterials*, vol. 30, no. 23-24, pp. 3801–3809, 2009.

[59] F. Scalera, C. Esposito Corcione, F. Montagna, A. Sannino, and A. Maffezzoli, "Development and characterization of UV curable epoxy/hydroxyapatite suspensions for stereolithography applied to bone tissue engineering," *Ceramics International*, vol. 40, no. 10, pp. 15455–15462, 2014.

[60] S. Oprea, S. Vlad, A. Stanciu, and M. Macoveanu, "Epoxy urethane acrylate," *European Polymer Journal*, vol. 36, no. 2, pp. 373–378, 2000.

[61] A. K. Antony, W. F. Chen, A. Kolokythas, K. A. Weimer, and M. N. Cohen, "Use of virtual surgery and stereolithography-guided osteotomy for mandibular reconstruction with the free fibula," *Plastic and Reconstructive Surgery*, vol. 128, no. 5, pp. 1080–1084, 2011.

[62] S. Bose, D. Ke, H. Sahasrabudhe, and A. Bandyopadhyay, "Additive manufacturing of biomaterials," *Progress in Materials Science*, vol. 93, pp. 45–111, 2018.

[63] Y. Huang, B. Cao, C. Xu, Q. Fan, and J. Shao, "Synthesis process control and property evaluation of a low-viscosity urethane acrylate oligomer for blue light curable ink of textile digital printing," *Textile Research Journal*, vol. 85, no. 7, pp. 759–767, 2014.

[64] B. W. Huang and M. Y. Chen, "Evaluation on some properties of SL7560 type photosensitive resin and its fabricated parts," *Applied Mechanics and Materials*, vol. 117-119, pp. 1164–1167, 2011.

[65] J. Stampfl, S. Baudis, C. Heller et al., "Photopolymers with tunable mechanical properties processed by laser-based high-resolution stereolithography," *Journal of Micromechanics and Microengineering*, vol. 18, no. 12, 2008.

[66] G. V. Salmoria, C. H. Ahrens, M. Fredel, V. Soldi, and A. T. N. Pires, "Stereolithography somos 7110 resin: mechanical behavior and fractography of parts post-cured by different methods," *Polymer Testing*, vol. 24, no. 2, pp. 157–162, 2005.

[67] Z. Weng, Y. Zhou, W. Lin, T. Senthil, and L. Wu, "Structure-property relationship of nano enhanced stereolithography resin for desktop SLA 3D printer," *Composites Part A: Applied Science and Manufacturing*, vol. 88, pp. 234–242, 2016.